American Mineralogist, Volume 71, pages 331–342, 1986

Quartz crystallization in igneous rocks

SAMUEL E. SWANSON
Geophysical Institute and Geology/Geophysics Program, University of Alaska, Fairbanks, Alaska 99701
PHILIP M. FENN
Sullivan Park FR-01-8, Corning Glass Works, Corning, New York 14831

ABSTRACT

Experiments on the growth of quartz from a variety of silicate melts show that the transition from euhedral to dendritic growth forms is dependent on the degree of undercooling (ΔT = temperature of the upper stability limit of quartz − temperature at which crystal growth begins) and is relatively independent of other variables such as bulk composition, pressure, or water content of the melt. Melts in the relatively simple system $NaAlSi_3O_8$-SiO_2-H_2O show the same pattern of quartz crystallization as those in more complex systems, such as Harding pegmatite + H_2O, but the kinetics are faster in the less viscous Harding melts. Euhedral crystals of quartz develop with small amounts of undercooling (ΔT < 55°C); dendritic quartz develops with greater amounts of undercooling. Measured growth rates parallel to the **c** axis are two to three times greater than those measured along the **a** axis. The highest measured growth rate was 7×10^{-8} cm/s at ΔT = 186°C in the Harding composition. Dendritic quartz is thus elongate along the **c** axis, a morphology that is commonly observed in igneous rocks. Skeletal quartz in igneous rocks is known from volcanic and subvolcanic environments and from pegmatitic systems. Undercooling required to produce these dendritic crystals (at least 55°C) may be caused by movement of magma to higher levels in the crust in the volcanic systems, by loss of volatiles, or by constitutional supercooling related to crystallization kinetics in the pegmatitic systems.

INTRODUCTION

In igneous rocks, quartz is found in a variety of textures reflecting not only the sequence of crystallization in a particular igneous system, but also the kinetics of crystallization. The texture of anhedral grains of quartz within a granular feldspar matrix is probably the most common form of quartz in igneous rocks and results from the late crystallization of quartz filling in between pre-existing feldspars. Subhedral to euhedral quartz grains found in igneous rocks reflect initiation of quartz crystallization before, at about the same time, or slightly after the beginning of feldspar crystallization. When quartz crystallizes early in an igneous system, there is ample space for the crystals to develop, and euhedral or subhedral grains result. Intergrowths of quartz and feldspar, such as those found in the graphic granite texture (Barker, 1970; Fenn, 1986), are the result of favorable crystallization kinetics in a given system. Variables that influence intergrowth development include the crystallization kinetics of quartz and feldspar, bulk composition, composition of the silicate liquid adjacent to growing crystals, and mobility of components within the silicate liquid.

To understand textural development of quartz in igneous rocks, the kinetics and sequence of crystallization must be understood for any given system. Phase-equilibria studies in a number of silicate systems provide basic information on crystallization sequence. However, relatively few studies are available on the kinetics of quartz crystallization in igneous systems. The purpose of this study is to describe the textures and kinetics of quartz crystallization observed in experiments in a number of systems and then to apply these results to quartz textures in igneous rocks.

PREVIOUS STUDIES OF QUARTZ CRYSTALLIZATION

Crystallization kinetics of SiO_2 (cristobalite is the normal crystalline product) from SiO_2-rich glasses have been studied by several workers (Brown and Kistler, 1959; Wagstaff, 1968, 1969; Christensen et al., 1973). These studies are of interest to materials scientists because the high-temperature use of SiO_2-rich glasses is limited by crystallization, but such work also offers some insight to the development of textural varieties of crystalline SiO_2 and crystallization kinetics, albeit in rather simple systems. Crystallization of cristobalite from pure SiO_2 glasses is one of the few instances in glass-forming systems where crystals grow from a solution (glass in this case) that has the same composition. Studies on crystallization kinetics in such systems furnish rather easily interpreted data on the mechanism of crystal growth. Wagstaff (1968, 1969) has studied the crystallization of cristobalite from pure SiO_2 and found that the cristobalite which nucleated entirely within the glass formed euhedral crystals. Growth rates for the internally nucleated cristobalite were independent of time, and reduced growth rates showed no variation with undercooling (ΔT); these observations indicated a continuous growth mechanism (Kirkpatrick, 1975). Other workers, such as Fenner (1913) and Christensen et al. (1973), have studied the crystallization kinetics of cristobalite in SiO_2-rich, but not pure, systems. Growth rates of cristobalite in these systems were also linear with time,

0003–004X/86/0304–0331$02.00

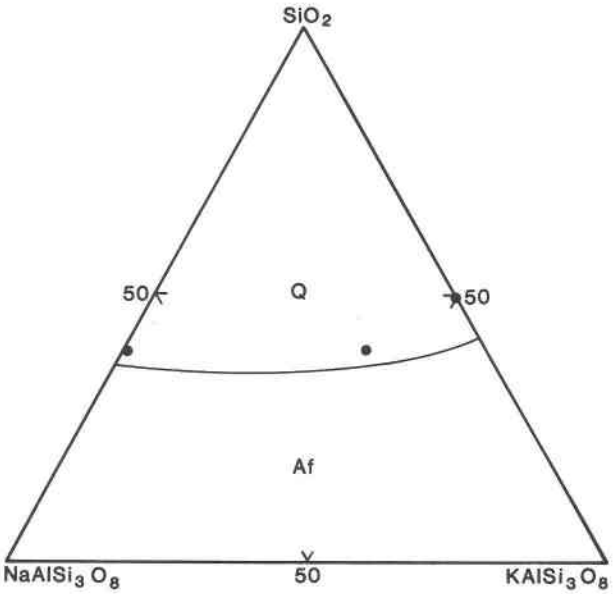

Fig. 1. Vapor-saturated liquidus phase diagram in the system $NaAlSi_3O_8$-$KAlSi_3O_8$-SiO_2-H_2O at 2 kbar (Tuttle and Bowen, 1958). Dots indicate bulk compositions (weight percent) used in this study.

indicating a continuous growth mechanism. However, the crystals of cristobalite had a dendritic habit. Compositional gradients detected in the silicate melt immediately adjacent to the cristobalite indicated an enrichment in the non-cristobalite-forming components resulting in a cellular crystal-liquid interface and thus producing dendritic cristobalite (Christensen et al., 1973).

Relatively few studies have dealt with the crystallization of quartz from geologically relevant systems. Lofgren (1971) reported the growth of quartz from natural rhyolitic glass during devitrification experiments. A micropoikilitic texture of subspherical quartz crystals surrounding feldspar fibers was developed best between 400 and 650°C at pressures less than 3 kbar from rhyolitic glass, whereas at 4 kbar, quartz formed pyramidally terminated prisms in devitrified rhyolite (Lofgren, 1971). Mustart (1972) grew crystals of quartz from melts in the system $Na_2Si_2O_5$-SiO_2-H_2O at a pressure of 4 kbar. At 650°C, doubly terminated bipyramids of β-quartz were obtained, and rhombs or scalenohedra of α-quartz were grown at 400°C. Quartz crystals can be grown directly from synthetic granitic liquids as illustrated by Swanson (1977). The quartz crystals show smooth, well-developed prism and pyramidal faces. Growth velocities along the **c** crystallographic axes were observed to be greater than growth rates on the **a** axes (Swanson, 1977).

Table 1. Compositions of starting materials

	Harding	Spruce Pine	R5
SiO_2	75.24	73.79	70.34
TiO_2	0.05	0.05	0.00
Al_2O_3	14.42	15.11	18.00
Fe_2O_3	0.14	0.26	0.00
FeO	0.35	0.16	0.00
MnO	0.18	0.05	0.00
MgO	0.01	0.07	0.00
CaO	0.20	0.97	3.97
Na_2O	4.23	4.71	4.37
K_2O	2.74	4.02	3.32
P_2O_5	0.13	0.01	0.00
F	0.64	0.01	0.00
CO_2	0.03	0.02	0.00
Total	93.36	99.23	100.00

Table 2. Definitive experiments for liquidus determinations in the system $NaAlSi_3O_8$-$KAlSi_3O_8$-SiO_2-H_2O

	P (kb)	T (°C)	X_{H_2O} (wt%)	time (hrs)	results
$Ab_{60}Q_{40}$					
	2.5	850	3.85	96	L
	2.5	900	3.21	72	L
	2.5	925	3.00	72	Xls+L
	2.5	925	3.85	72	L
	2.5	950	2.76	72	L
	2.5	1000	0.99	96	Xls+L
	2.5	1000	2.00	96	L
	5.0	800	7.99	240	Xls+L
	5.0	900	5.00	72	Xls+L
	5.0	900	6.00	72	L
	5.0	1000	3.00	72	Xls+L
	5.0	1000	3.99	72	L
	8.0	1000	5.99	96	Xls+L
	8.0	1000	8.05	96	L
	8.0	1100	3.83	48	Xls+L
$Ab_{50}Q_{50}$					
	8.0	1000	7.99	96	Xls+L
	8.0	1000	8.94	96	L
	8.0	1100	5.01	48	Xls+L
$Ab_{40}Q_{60}$					
	8.0	1100	5.01	48	Xls+L
	8.0	1100	9.99	48	L

Experimental methods

Three compositions in the primary phase field of quartz in the system $NaAlSi_3O_8$-$KAlSi_3O_8$-SiO_2 (Fig. 1) were prepared as dehydrated silicate gels (Luth and Ingamells, 1965). Another bulk composition that represents a synthetic granodiorite (composition R5, Table 1) in the system $NaAlSi_3O_8$-$KAlSi_3O_8$-$CaAl_2Si_2O_8$-SiO_2-H_2O has been previously studied (Whitney, 1975; Swanson, 1977) and crystallizes quartz after the growth of plagioclase and alkali feldspar. Natural starting materials are represented by pegmatite samples from the Spruce Pine district (North Carolina) and from the Harding pegmatite (New Mexico) (Table 1).

Phase relations in the system $NaAlSi_3O_8$-$KAlSi_3O_8$-SiO_2-H_2O were extracted from a number of sources including Luth et al. (1964) and Luth (1969). A limited number of phase-equilibria experiments were done on the composition $Ab_{60}Q_{40}$ (weight percent) to check predicted phase relations. Results of some of these experiments are shown (Table 2, Fig. 2) and confirm the predicted phase relations.

Experimental techniques have been described previously (Fenn, 1977; Swanson, 1977, 1979). Briefly, a measured amount of silicate (20–30 mg) is added to water in a noble metal capsule (2.0 mm O.D.). After sealing, capsules were placed in an internally heated pressure vessel. Pressure and temperature were adjusted and maintained during the phase-equilibria experiments. For crystal-growth experiments, pressure and temperature were adjusted to bring the system above the liquidus (T_L) for times (t_L) of not less than 72 h. Temperature and pressure conditions were

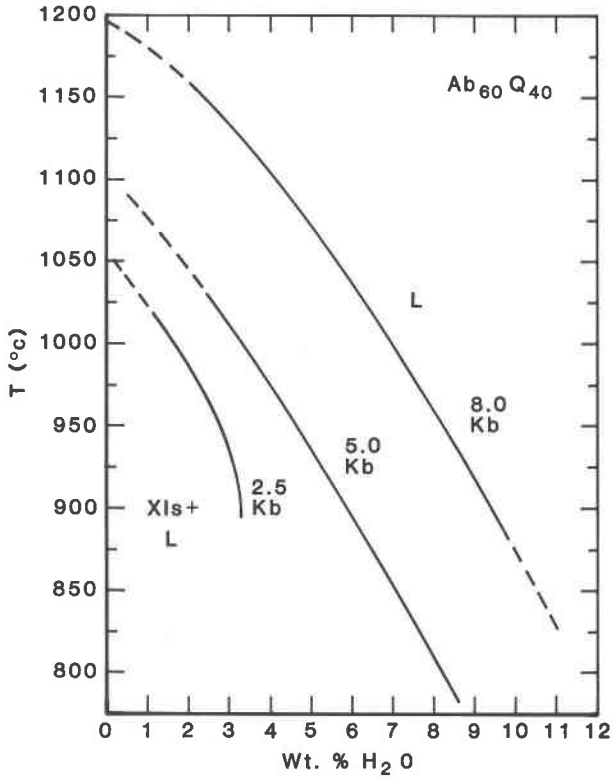

Fig. 2. Vapor-undersaturated phase relations for $Ab_{60}Q_{40}$ (weight percent) at 2.5, 5.0, and 8.0 kbar. Diagram is based on literature data (Luth et al., 1964; Luth, 1969) and on the results in Table 2.

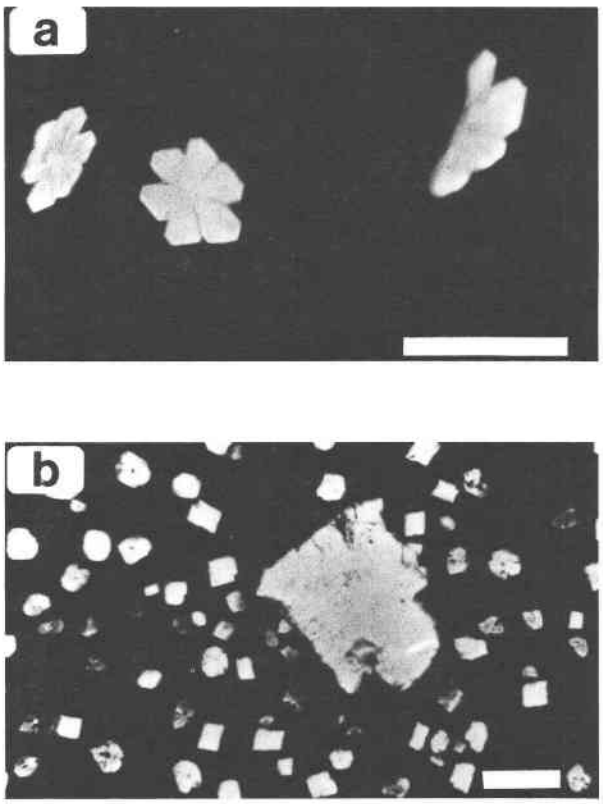

Fig. 3. Photomicrographs of euhedral to subhedral quartz grown at low degrees of undercooling (ΔT). White bar in all photos is 0.10 mm long. (a) R5 + 6.5 wt% H_2O. P = 8 kb, T_L = 900°C, t_L = 96 h; T_G = 650°C, t_G = 48 h; ΔT = 35°C. Hexagonal plates of α-quartz. (b) Harding + 7.5 wt% H_2O. P = 5 kb, T_L = 900°C, t_L = 72 h, T_G = 650°C, t_G = 240 h, $\Delta T_{\alpha\text{-quartz}}$ = 55°C. Euhedral bipyramids of α-quartz surround a larger albite crystal. T_L = temperature of liquid generation, t_L = time of liquid generation, T_G = temperature of crystal growth, t_G = time of crystal growth.

readjusted to the temperature selected for crystal nucleation and growth (T_G). The time required for temperature readjustment was on the order of minutes, and pressure was readjusted following the drop in temperature. Samples remained at the growth temperature for times (t_G) of 6 to 500 h and were then quenched to room temperature by turning off the furnace power. Capsule weight was checked before and after each experiment to ascertain that each capsule acted as a closed system during the experiment.

Results

Morphology

The morphology of quartz grown in the dynamic crystallization experiments of this study can be directly correlated with the degree of undercooling (ΔT = temperature of the upper stability of quartz − temperature of experiment). For small amounts of undercooling (20–55°C), quartz forms single euhedral crystals; high-temperature β-quartz typically forms subhedral to euhedral hexagonal plates (Fig. 3a). Low-temperature α-quartz produces isolated bipyramids when undercooled more than 100°C (Fig. 3b). The euhedral habit of α-quartz crystals may seem anomalous in light of the much smaller degree of undercooling required to produce euhedral β-quartz. However, for the experiment in Figure 3b, the δ-β quartz transition is between the liquidus temperature and the temperature of the experiment. Thus, the $\Delta T_{\beta\text{-quartz}}$ is 111°C for this experiment, whereas the $\Delta T_{\alpha\text{-quartz}}$ defined by the metastable α-quartz liquidus is lower. The euhedral α-quartz is produced at a low ΔT defined by the metastable α-quartz liquidus. This complication is not found in the other experiments, since the α-β transition does not occur within the experiments.

Dendritic crystals of quartz are produced in dynamic crystallization experiments when ΔT is greater than about 55°C (Fig. 4). Dendrite arms develop parallel to the **a** and **c** crystallographic axes with smaller dendrite arms branching off of these major axes of growth. Crystals are commonly elongate parallel to the **c** axis. When viewed down the **x** axis, the hexagonal symmetry of some of the dendrites resembles snow flakes (Swanson, 1977; Fig. 4c). At least some of the dendrite branches off the **a** axes parallel the prism directions in quartz (Fig. 4c). Quartz maintains the dendritic morphology illustrated in Figure 4 to the highest ΔT values (235°C) studied. The only noticeable change in dendrite morphology is from coarse-grained dendrites (Figs. 4a, 4b) at smaller ΔT values to finer-grained dendrites (Fig. 4c) at larger ΔT values. Variation

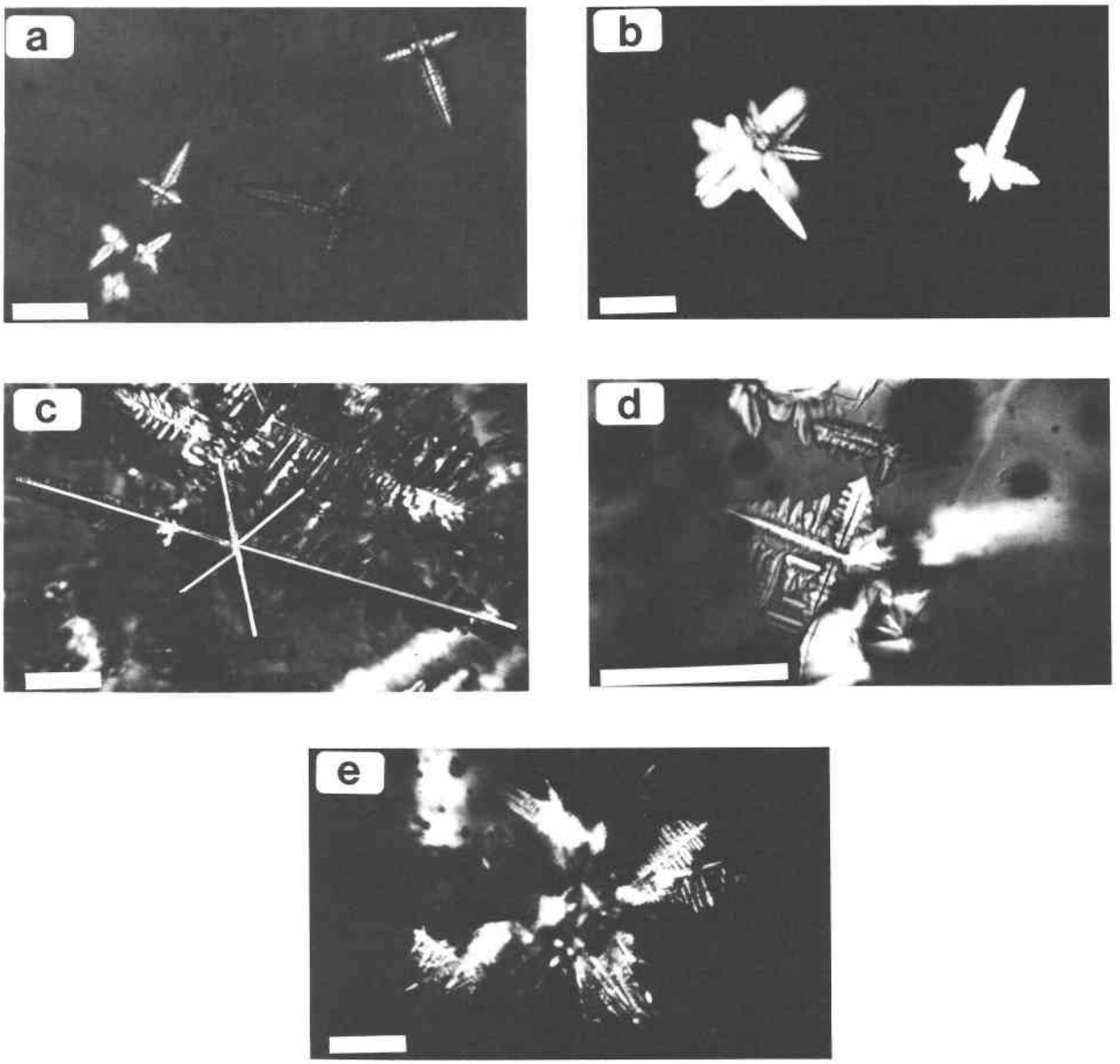

Fig. 4. Photomicrographs of dendritic β-quartz grown at high ΔT. White bar in all photos is 0.10 mm long. (a) $Ab_{60}Q_{40}$ + 3.99 wt% H_2O. P = 8 kbar, T_L = 1150°C, t_L = 72 h, T_G = 900°C, t_G = 120 h, ΔT = 105°C. Quartz is elongate parallel to the **c** axis, with smaller dendrite arms parallel to the **a** axis. (b) Harding + 4.5 wt% H_2O. P = 5 kb, T_L = 900°C, t_L = 72 h, T_G = 750°C, t_G = 96 h, ΔT = 136°C. Crystals as in (a). (c) $Ab_{60}Q_{40}$ + 5.01 wt% H_2O. Same conditions as in (a); ΔT = 165°C. Dendritic crystal viewed down the **c** axis showing hexagonal symmetry. Near-extinct crystal is emphasized with white lines. (d) $Ab_{20}Or_{40}Q_{40}$ + 4.03 wt% H_2O. P = 2 kbar, T_L = 1100°C, t_L = 72 h, T_G = 800°C, t_G = 120 h, $\Delta T \approx$ 120°C (phase relations poorly known). Dendritic quartz with well-developed facets. (e) $Or_{50}Q_{50}$ + 2.00 wt% H_2O. Same conditions as in (d); $\Delta T \approx$ 140°C (phase relations poorly known). Fine-grained quartz dendrites. Symbols as in Fig. 3.

in ΔT—rather than anhydrous bulk composition or pressure—produces the most dramatic changes in quartz morphology for the experiments in this study.

Variation in ΔT may be produced isothermally by changing the concentration of one or more components in the silicate liquid (Petersen and Lofgren, 1986). In silicate systems where the melt is undersaturated with respect to water, the liquidus temperature varies as a function of the water content of the system (Fig. 5): The lower the water content, the higher the liquidus temperature. Thus, the temperature of crystal growth can be held constant, but variation of water content and hence liquidus temperature will result in a variation in ΔT. Crystal morphology may show variation with water content at a particular isotherm, but the morphology change is related to the variation in ΔT with changing water content. Figure 6 shows quartz crystals grown at 700°C for 97 h with variable water content (4.5–6.5 wt%) and ΔT (61–186°C).

The pattern of crystallization illustrated in Figure 6 is similar to that in Figures 2 and 3. Euhedral crystals of quartz are found at the lowest ΔT (Fig. 6a). Skeletal crystals are found at intermediate ΔT (Figs. 6b, 6d). Dendritic crystals are found at the highest ΔT (Figs. 6e, 6f). Growth rate increases with the degree of undercooling as evidenced by the larger crystals at higher ΔT (Fig. 7).

Systems investigated in this study were selected to assess the roles of bulk composition and nature of the starting material on the growth of quartz. The Harding pegmatite sample is composed of natural material. Phase-equilibria studies on this natural system show that quartz is the liquidus phase. Quartz is also the liquidus phase in the bulk compositions studied in the system $NaAlSi_3O_8$-$KAlSi_3O_8$-SiO_2-H_2O, but the starting materials in this system were fixed silica gels. The synthetic granodiorite also used fixed silica gel as a starting material. However, plagioclase is the liquidus phase in this system, and alkali feldspar and quartz crystallize at lower temperatures. The morphology of quartz grown from these systems does not show any variation with bulk composition, despite the differences in phase relations and starting materials (Figs. 3, 4, and 6). However, the kinetics of the crystal growth are compositionally dependent, as discussed in the next section.

Within the limits of these experiments, pressure does not seem to influence the morphology of the dendritic quartz crystals (Figs. 3 and 4). Experiments with a composition $Ab_{60}Q_{40}$ and various water contents at 2000, 2500, 5000, and 8000 bars produce dendritic crystals of quartz. Analytical expressions for the rate of crystal growth and the diffusivity of components in the melt at the present do not contain a pressure term owing to a lack of data (Kirkpatrick, 1975). Silicate melts show a decrease in melt viscosity with increasing pressure (Kushiro, 1976); thus, a relation between crystallization kinetics (and hence morphology) and pressure would be expected.

Crystallization kinetics

Quartz crystals grown in this study show pronounced elongation parallel to the **c** and **a** crystallographic axes with the dimensions along **c** greater than those along **a**. This relation has been observed in other experimental studies of quartz crystallization (Swanson, 1977) and is the morphology commonly observed in natural crystals. Elongation parallel to one or more crystallographic axes indicates higher growth rates along them relative to other directions; for quartz, the growth rate along **c** is greater than the growth rate along **a**.

Crystallization kinetics are measured in this type of experiment by determining the amount of crystal growth as a function of time. Data commonly accumulated for each experiment includes the length of crystal growth as a function of crystallographic direction and the number of crystal nuclei present within an experiment. When combined with the duration of the experiment, these data describe the crystallization kinetics of the system. A more complete description of kinetic measurements in similar

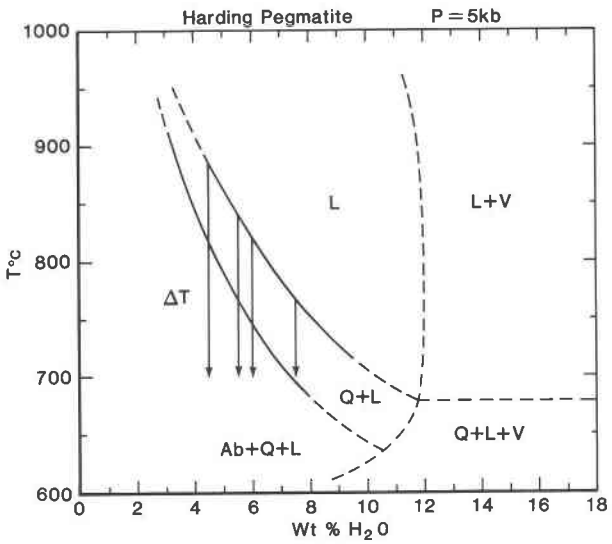

Fig. 5. Liquidus diagram for the Harding composition at P = 5 kbar. Arrows illustrate the range of ΔT values produced by a 3 wt% variation in water content. Experiments corresponding to each of the arrows are shown in Fig. 6. Dashed lines represent schematic phase relations.

systems and of the problems that affect these measurements is found in Fenn (1977) and Swanson (1977).

Crystal-growth kinetics for quartz in two of the bulk compositions studied are given in Figure 7. The amount of growth plotted on Figure 7 represents one-half the **a** or **c** dimension for the largest crystal in an experiment to account for crystal growth in two directions along the axes. The amount of time of growth plotted on Figure 7 is the period of time the experiment was held at the growth isotherm (t_G). Other studies such as Fenn (1977) and Swanson (1977) have shown that there may be a lag between the time of temperature drop to a growth isotherm and the nucleation of crystals (nucleation lag time) and that growth rates measured using t_G will give minimum values. Nucleation lag times were not determined for most of the compositions in the present study, and the reported growth rates are thus minimum growth rates.

Crystal-growth rate is equal to the slope of the curve on a crystal growth vs. time plot, such as Figure 7. For the $Ab_{60}Q_{40}$ composition at either 900 or 850°C, only two data points define the growth rate and the relationship shown is, of course, linear. Without any additional data, the growth rates shown on Figure 7b are certainly questionable. However, some experiments did not nucleate any crystals, and these results are at least consistent with the growth rates shown. At 900°C an experiment of 48-h duration did not nucleate any crystals, but an experiment held at 900°C for 72 h did nucleate crystals of quartz (Table 3); thus, a nucleation lag time for this composition is 60 ± 12 h at 900°C. Intersection of the growth rates for the **c** and **a** axes at 900°C is at about 60 h for zero growth; thus, a nucleation lag time for this composition is about 60 h at 900°C. The 48-h experiment at 900°C

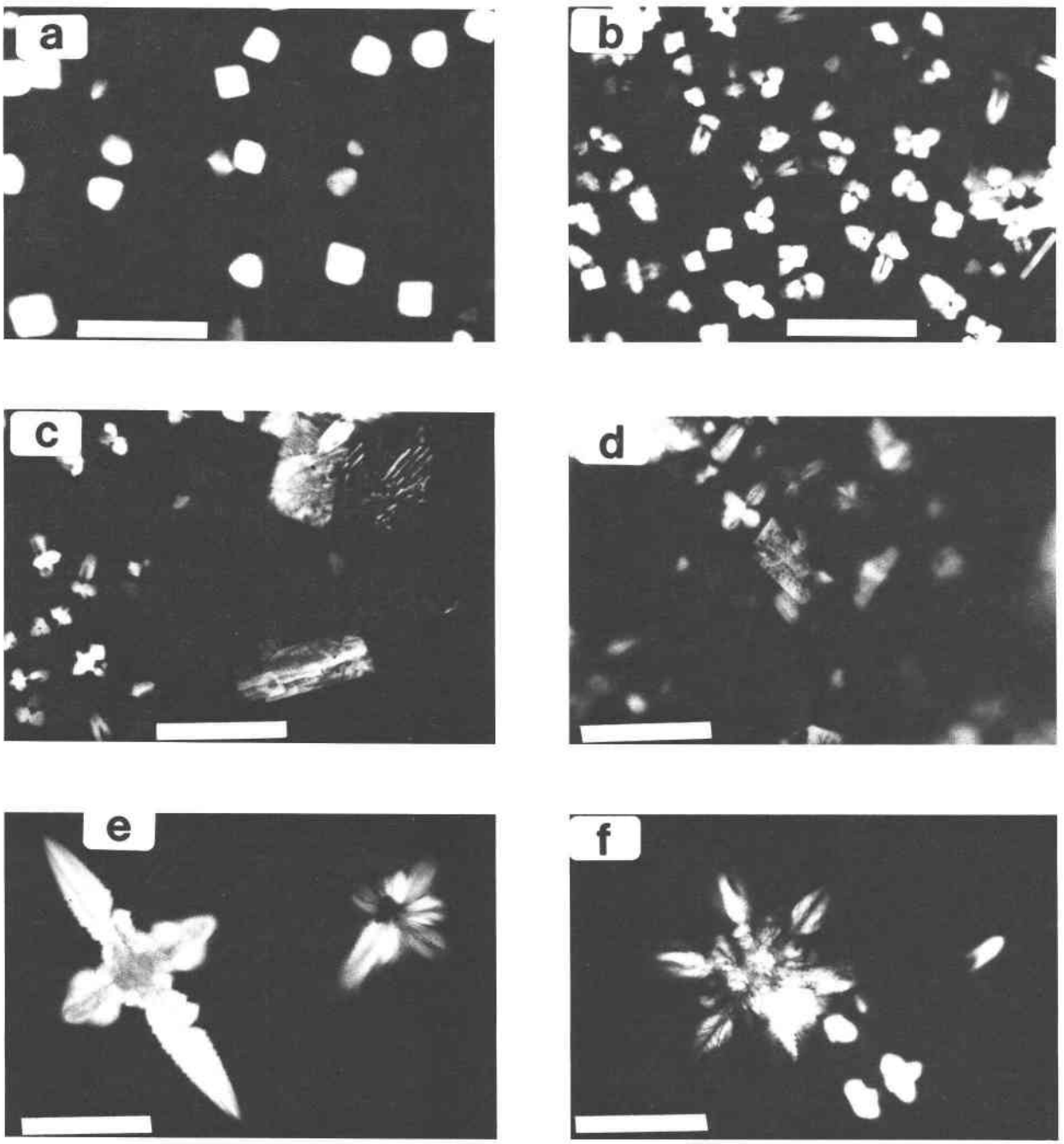

Fig. 6. Quartz grown in the Harding composition at $P = 5$ kbar, $T_L = 900°C$, $t_L = 72$ h, $T_G = 700°C$, $t_G = 97$ h with variable water contents. White bar in all photos is 0.5 mm long. (a) Harding + 6.5 wt% H_2O, $\Delta T = 61°C$. Euhedral bipyramids of quartz. (b) Harding + 6.00 wt% H_2O, $\Delta T = 101°C$. Subhedral "hopper" bipyramids of quartz. (c) Same as (b), but including some quartz-feldspar intergrowths. (d) Harding + 5.50 wt% H_2O, $\Delta T = 140°C$. Small dendritic quartz crystals surrounded by larger albite crystals. (e) Harding + 4.50 wt% H_2O, $\Delta T = 186°C$. Quartz dendrites elongate along the c axis. (f) Same as (e) showing hexagonal symmetry.

that did not nucleate crystals is consistent with this prediction. Experiments held at 850°C for 6 and 24 h did not nucleate any crystals, but an experiment of 48-h duration did nucleate crystals (Table 3) for a nucleation lag time of 36 ± 12 h. The growth rates at 850°C suggest a value for the nucleation lag time of about 36 h, identical, within the limits of the data, to the value predicted from the crystal-growth experiments. Thus, although the growth rates for $Ab_{60}Q_{40}$ are derived from a limited data base, they are consistent with all of the experimental results.

Growth-rate data for quartz in the Harding composition are comparatively abundant and do not show a linear

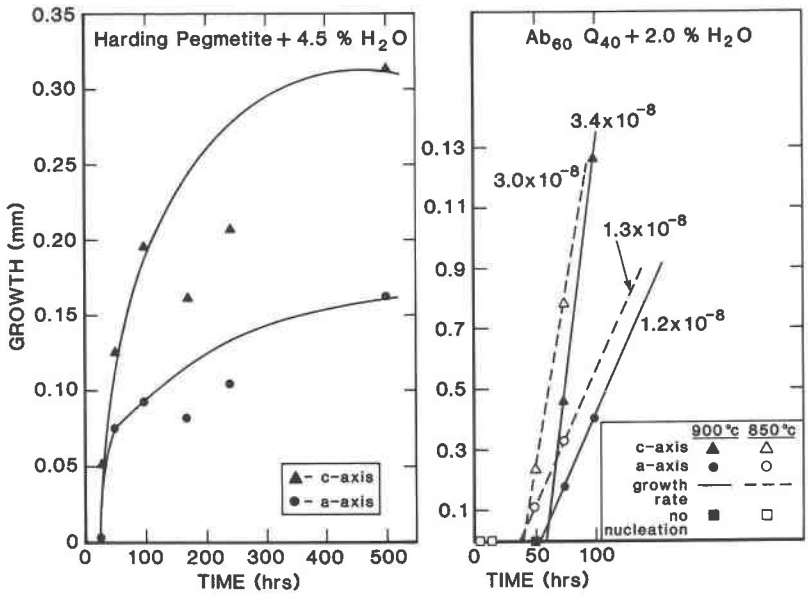

Fig. 7. Growth kinetics of quartz as a function of crystallographic direction. Data are given in Table 3. (a) Harding + 4.5 wt% H_2O. P = 5 kbar, T_L = 900°C, t_L = 72 h; T_G = 750°C. (b) $Ab_{60}Q_{40}$ + 2.0 wt% H_2O. P = 2.5 kbar, T_L = 1000°C, t_L = 72 hr. Numbers on lines are linear growth rates in cm/s.

relation on a growth vs. time plot. Indeed, growth rates measured in this system seem to decrease with increasing time (Fig. 7a). The maximum growth rate observed in this system (7.3×10^{-8} cm/s) is defined by growth along the **c** axis in the experiments of 24 and 48 h. Using these experiments to define the growth rate yields a nucleation lag time of about 6 h. Growth rates calculated from the 24- and 48-h data along the **a** axis are approximately the same (7.9×10^{-8} cm/s) as those along the **c** axis. However, this value for the growth rate along **a** is thought to be too high because (1) the calculated growth rates along the **a** and **c** axes are approximately the same yet the crystals are elongate along the **c** axis, a fact that suggests faster growth in this direction, and (2) the slopes of the growth rates are approximately parallel and this parallelism is not consistent with a nucleation lag time of about 6 h. For these reasons the initiation of crystal growth along the **a** axis is *assumed* to have started at the same time as growth along the **c** axis; thus, the growth rate along **a** is preferably interpreted as 4.3×10^{-8} cm/s. Several experiments were duplicated to allow for the probabilistic nature of nucleation in these systems (Fenn, 1977; Swanson, 1977), but for the duplicates, only the maximum value was used to construct the growth-rate curve. Experiments at 168 and 240 h do not fall on the curve defined by the maximum observed growth in the other experiments (Fig. 7a).

Measured crystal-growth rates along the **c** axis in quartz are greater than growth rates measured along the **a** axis in all of the compositions studied. Figure 8 shows that for both the $Ab_{60}Q_{40}$ and Harding compositions, the rate of growth measured along the **c** axis (e.g., $Ab_{60}Q_{40}$ yielded 3.0 to 3.4 $\times 10^{-8}$ cm/s) is about twice as large as growth rates measured along the **a** axis (e.g., $Ab_{60}Q_{40}$ yielded 1.2 to 1.3 $\times 10^{-8}$ cm/s. This relation appears independent of ΔT, at least in the temperature interval investigated. The faster growth rate along the **c** axis results in quartz crystals that are elongate parallel to the **c** axis, a texture that is commonly found in our experimental products (Figs. 3, 4, and 6) as well as in natural quartz.

The rate of crystal growth for a particular phase is largely a function of temperature (commonly expressed as ΔT).

Table 3. Selected kinetic data for quartz

Harding Pegmatite + 4.5 wt % H_2O*

Time (hrs)	length of growth (in mm) parallel to a	c
24	0.002	0.051
48	0.075	0.126
96	0.092	0.196
168	0.081	0.161
240	0.104	0.207
500	0.161	0.333

$Ab_{60}Q_{40}$ + 2.0 wt % H_2O**

Time (hrs)	length of growth (in mm) parallel to a	c
48	no nucleation	
72	0.017	0.046
96	0.040	0.116

$Ab_{60}Q_{40}$ + 2.0 wt % H_2O***

Time (hrs)	length of growth (in mm) parallel to a	c
6	no nucleation	
24	no nucleation	
48	0.0116	0.0232
72	0.0325	0.0780

* P = 5.0 kb; experiments held at 900°C for 72 hrs prior to crystal growth at 750°C.
** P = 2.5 kb; experiments held at 1000°C for 72 hrs prior to crystal growth at 900°C.
*** P = 2.5 kb; experiments held at 1000°C for 72 hrs prior to crystal growth at 850°C.

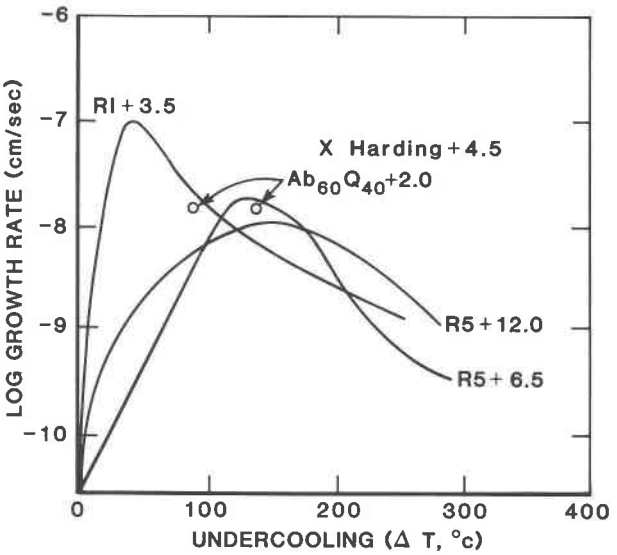

Fig. 8. Growth rate of quartz measured parallel to the c axis in various systems as a function of undercooling. Harding and $Ab_{60}Q_{40}$ data from Fig. 7. R5 + 6.5 wt% H_2O, R5 + 12 wt% H_2O, and R1 (synthetic granite) + 3.5 wt% H_2O are from Swanson (1977).

Quartz growth rates measured in the $Ab_{60}Q_{40}$ composition show little variation over an undercooling range of 50°C (Fig. 7b). However, Swanson (1977) has shown that the growth rate of quartz in granitic systems varies by several orders of magnitude over a ΔT range of 300°C. For comparison, Swanson's data are shown in Figure 8 together with the maximum growth rates for the $Ab_{60}Q_{40}$ and Harding compositions from Figure 7. Growth rates in the $Ab_{60}Q_{40}$ composition are comparable to results in the granitic systems at equivalent degrees of undercooling. In contrast, quartz crystallized from the Harding composition has a higher growth rate, at a ΔT of 136°C, than quartz crystallized from any of the other bulk compositions studied.

No attempt was made in the present study to quantify nucleation kinetics. Swanson (1977) has presented data for the nucleation of quartz in haplogranitic compositions as a function of ΔT. Nucleation in the systems studied is clearly related to ΔT as shown by an increase in the number of nuclei with increasing ΔT (at some constant experiment duration) and a decrease in the nucleation lag time. For example, nucleation lag time in the $Ab_{60}Q_{40}$ composition decreases from 60 to 36 h as the ΔT increases from 85 to 135°C (Fig. 7b). Nucleation lag times appear to be shortest for the Harding composition, at any given ΔT, relative to the other systems studied. Results at $\Delta T \approx$ 135°C (Fig. 7) yield nucleation lag times of 36 h for the $Ab_{60}Q_{40}$ system and 6 h for the Harding composition.

Discussion of experimental results

The transition from euhedral crystals of quartz at relatively small degrees of undercooling to dendritic morphologies at larger degrees of undercooling is caused by a breakdown of planar crystal faces during growth. A crystal growing from a melt of different composition will induce thermal and compositional irregularities in the boundary layer in the melt adjacent to the growing crystal (Kirkpatrick, 1981). The net effect of the accumulation of heat from crystallization and of noncrystallizing components in the boundary layer is to reduce the planar growth rate of the crystal. The growth rate of any projection into the boundary layer will be enhanced relative to the growth of the planar crystal face; the result is a transition from a crystal with smooth faces to a crystal with a cellular morphology. Once instabilities are developed on a crystal face, they become self-perpetuating because the larger surface area to volume ratio of the instabilities produces a larger ΔT at the crystal interface (R. J. Kirkpatrick, personal communication, 1985). Instabilities in silicates found at moderate ΔT values commonly have some specific crystallographic orientation, and the instabilities are terminated by crystal faces (termed facets) (Kirkpatrick, 1975). Development of instabilities along the **a** and **c** crystallographic directions in quartz has resulted in dendritic morphologies (Figs. 4 and 6). All of the dendrite arms (instabilities) in the quartz down to the lowest temperatures studied (ΔT = 235°C) are faceted, a result expected from the anisotropic growth rates of quartz (O'Hara et al., 1968). Facets appear to correspond to the prism faces on quartz. Spacing between the instabilities in the quartz dendrites decreases with increasing ΔT (Fig. 6) owing to the reduced mobility of the noncrystallizing components at lower temperature (Keith and Padden, 1963; Kirkpatrick, 1975).

Growth rates of quartz taken from Figure 7b show a decrease (at constant temperature) with increasing duration of growth. Another approach used in measuring growth rates in similar systems was employed by Fenn (1977) and Swanson (1977) where the maximum amount of crystal growth in an experiment was divided by the duration of the experiment to determine the growth rate. Growth rates so measured on the Harding quartz (Fig. 7b) are given on Figure 9, which clearly shows the time dependence of the growth rate in these experiments. For experiments of short duration (up to 48 h), the growth rate shows an apparent increase with duration, but then the growth rate decreases with time in experiments of longer duration (Fig. 9). The initial apparent increase in growth rate with increasing time is probably related to the nucleation lag time, an effect that is especially important in short-duration experiments. If the duration of the growth period for the Harding quartz crystals is reduced by 6 h to compensate for the nucleation lag time, the initial increase in the growth rate is almost eliminated (Fig. 9). Another result of this recalculation is the apparent consistency of the data at 168- and 240-h duration. These data fall well below the maximum growth-rate curve on an amount of growth vs. time plot (Fig. 7a), but now appear to be part of a trend of decreasing growth rate with increasing time.

Theoretical models for the growth of crystals from silicate melts predict that crystal-growth rate for faceted

crystals should be independent of time (Kirkpatrick, 1975), whereas the diffusion-controlled growth rate of dendrites is inversely dependent on time. In systems where the equilibrium proportion of a crystalline phase is less than 100%, the growth rate may be expected to decrease as the crystalline proportion approaches an equilibrium value. The decrease in growth rate with time (Fig. 9) may be ascribed to an approach to equilibrium, the time-dependent behavior of diffusion-controlled growth, or a combination of both causes. Crystal-growth rates for the Harding composition are greater, at a particular ΔT, than growth rates in other systems (Fig. 8). The 6-h nucleation lag time for quartz in the Harding composition (Fig. 7b) is as short, if not shorter, than nucleation lag times measured in the other systems we have studied. Viscosity calculations, based on the method of Shaw (1972), for the compositions studied over the reported range of temperature and water content show that melts of the Harding composition have lower viscosities than any other composition. The faster crystallization kinetics reported for the Harding composition are probably related to greater mobility of components in the silicate liquid because of the lower viscosities of these melts.

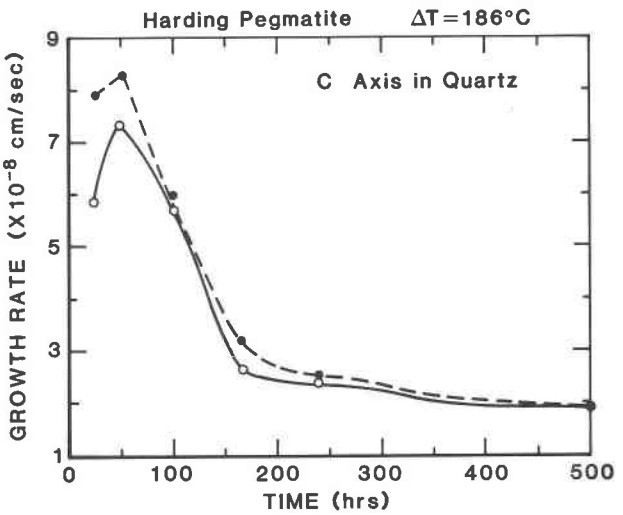

Fig. 9. Growth rate as a function of time for the Harding data in Table 3 and Fig. 7. Growth rates were calculated assuming a linear growth rate with (●) and without (○) correction for nucleation lag time.

Applications

Texture of quartz in igneous rocks is controlled by the crystallization order of quartz relative to the other rock-forming minerals. In most igneous systems, quartz crystallization follows the growth of one or more rock-forming minerals resulting in quartz growth in a confined space. Mutual interference of quartz and these early-formed phases results in the equidimensional, anhedral grains of quartz commonly observed in plutonic rocks. Subhedral and euhedral quartz grains are usually restricted to volcanic or hypabyssal plutonic rocks where the phenocrysts of quartz develop without interference from adjacent grains. Deep-seated plutonic rocks may also contain subhedral to euhedral quartz, but in such cases the form is clearly related to the relatively early crystallization of quartz.

Experimental results indicate that equigranular forms of quartz crystallize at a low ΔT, probably on the order of 55°C or less, whereas crystallization at higher ΔT results in dendritic forms. Crystallization at low ΔT indicates that the igneous system was undergoing slow cooling. Low cooling rates do not produce the thermal or compositional irregularities that promote high ΔT and hence dendrites. An upper limit can be placed on the cooling rate required to produce nondendritic quartz by using the limiting conditions of ΔT = 55°C and nucleation lag time = 24 h (typical over the ΔT range our experiments). Melts that are undercooled more than 55°C in less than 24 h will crystallize dendritic quartz crystals, and thus the limiting cooling rate between dendritic and nondendritic quartz is about 55°C/24 h (~2°C/h). Lower cooling rates will yield nondendritic crystals; higher cooling rates will result in dendritic crystals.

Volcanic phenocrysts

Quartz phenocrysts in volcanic or hypabyssal plutonic rocks are often embayed (Fig. 10). The embayed crystals may have reaction coronas indicating reaction of the silicate liquid with the quartz resulting in partial dissolution (embayment) of a previously subhedral to euhedral quartz phenocryst. However, many embayed quartz crystals show no evidence of a reaction relation and are often enclosed by a groundmass that also contains quartz. In such cases, evidence for quartz dissolution is less clear, and the "embayed" crystals may represent primary skeletal crystals. Some crystals occasionally show crystallographic control of the "embayment"; preferential underdevelopment of the prism faces results in crystals similar to some of the dendritic forms grown in the present study (compare Figs. 3a and 10).

Unidirectional solidification textures

Dendritic quartz from shallow-level granite stocks in the Henderson molybdenum deposit in Colorado has been described by Shannon et al. (1982). These dendrites are associated with layers of quartz and alkali feldspar. The layers are monomineralic or are composed of alkali feldspar–quartz intergrowths with crystal terminations that project toward the interior of the stock and form unidirectional solidification textures (Shannon et al., 1982). Fine-grained aplitic granite fills the space between individual crystals and between the layers. Crystal form in the layers ranges from euhedral to dendritic, and the transition between euhedral and dendritic forms is typically abrupt (Fig. 11). The layers are concordant to the contacts of the stocks, and this pattern along with the crystal form suggests that the layers formed at a crystal-liquid interface during the inward crystallization of the stocks. The transition from euhedral to dendritic quartz observed in some

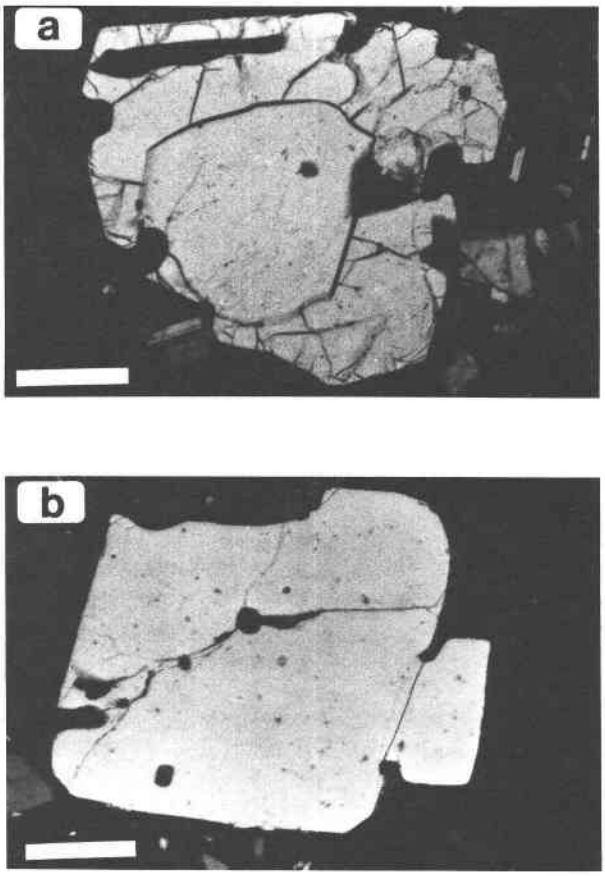

Fig. 10. Skeletal quartz phenocrysts in volcanic rocks. White bar in both photos is 0.5 mm long. (a) Quartz in dacite from Kaguyak Crater, Katmai National Park, Alaska. (b) Quartz in Mitchell Mesa rhyolite, west Texas.

of the layers suggests that undercooling increased during crystallization of those layers. Results of our experiments show that a minimum undercooling of 55°C is required to produce dendritic quartz and suggest that the layers with euhedral to dendritic quartz at Henderson experienced an event that produced an undercooling of at least 55°C during crystallization. Aplitic textures that follow dendrite crystallization (Fig. 11) are also consistent with formation at high degrees of undercooling (many nucleation sites, low growth rate; Swanson, 1977). In the Henderson stocks, numerous layers with repeated unidirectional solidification textures (Shannon et al., 1982) show that the euhedral to dendritic transition occurred many times during crystallization. The Henderson stocks formed by crystallization of a vapor-saturated granitic magma at shallow levels in the crust (White et al., 1981). Periodic venting of a vapor phase during crystallization of the stocks may explain the periodic undercoolings that produced the euhedral to dendritic textures in layers of the Henderson stocks.

Dendritic quartz in pegmatites

Well-developed dendritic quartz is found in zones adjacent to some large pegmatite cores from the Spruce Pine

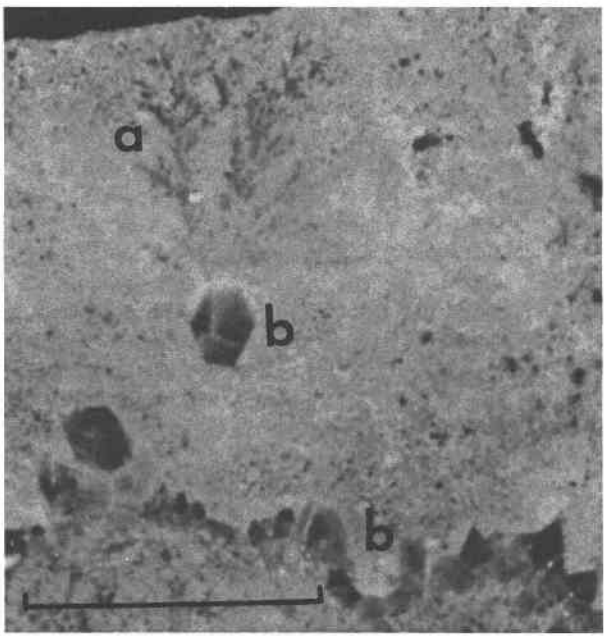

Fig. 11. Dendritic quartz (a) associated with euhedral quartz layer (b) from the Henderson stocks, Colorado. Fine-grained, gray aplitic granite surrounds the quartz. Scale = 2 cm.

district of North Carolina (Swanson, 1978a, 1978b). Spruce Pine pegmatites are zoned from a margin of plagioclase + potassium feldspar + quartz + white mica to a core of quartz + potassium feldspar (Cameron et al., 1949). Immediately adjacent to the core is a zone of plagioclase + potassium feldspar + dendritic quartz (Fig. 12). The dendritic quartz is generally elongate parallel to the **c** crystallographic axis and shows a pinnate texture of dendrite arms branching from the **c** axis (Fig. 12). Many of these dendrite arms are found to be parallel to the **a** axis. Similar observations of textural variation in quartz have been made in other pegmatites (Jahns, 1955). Maurice (1940) proposed a replacement origin for the skeletal quartz in the Spruce Pine feldspars. However, the textures are very similar to those produced in this study, and we believe that the dendritic quartz represents a primary crystallization product.

Crystallization experiments with a Spruce Pine composition (Table 1) have produced crystals of dendritic quartz (Fenn, 1986). Plagioclase is the liquidus phase in this system, and quartz is the second phase to crystallize (at 5 kbar, the pressure of the experiments). Quartz crystallized at $\Delta T = 65$°C is dendritic, but smaller degrees of undercooling do not nucleate quartz (Fenn, 1986).

The association of dendritic quartz in the Spruce Pine pegmatites with skeletal feldspar and white mica (Swanson, 1978a) suggests crystallization in an undercooled environment. Spruce Pine pegmatites do not show abundant evidence (aplitic textures, miarolitic cavities) for vapor-phase evolution during their crystallization. Thus, loss of a vapor phase is probably not responsible for the ΔT that resulted in crystallization of dendritic quartz and skeletal feldspar and mica in the Spruce Pine system.

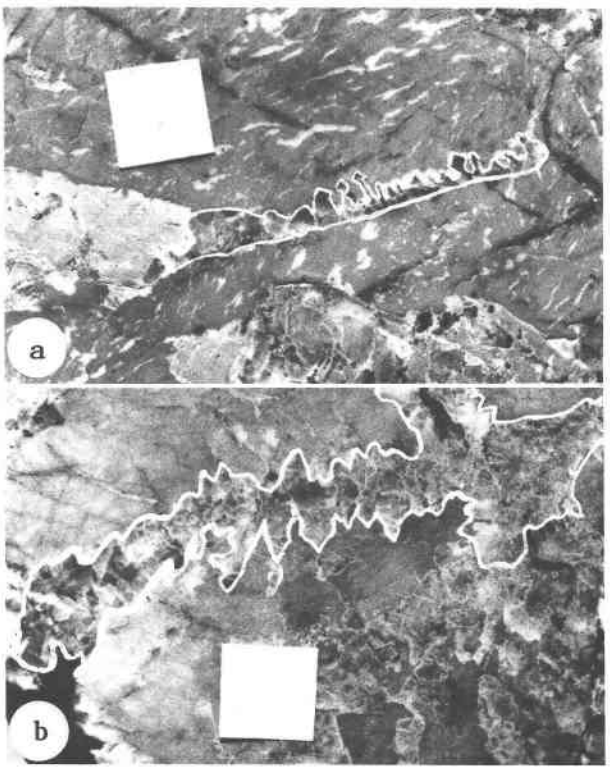

Fig. 12. Dendritic quartz in feldspar from the McKinney mine, Spruce Pine, North Carolina (Swanson, 1978a, 1978b). White square is 1.0 cm². Quartz is elongate parallel to the c axis. (a) Quartz in K-feldspar host. (b) Quartz in plagioclase host.

Mineral zoning within the Spruce Pine pegmatites suggests that a compositional gradient was present during pegmatite crystallization. Constitutional supercooling associated with the compositional gradient, perhaps accentuated by rapid crystallization kinetics, may be responsible for the zone of undercooling. The intermediate position of the undercooled zone (and quartz dendrites) within the pegmatites is consistent with such an origin. The dendritic habit of the quartz suggests that the undercooling was at least 55°C, on the basis of the results of this study.

Conclusions

Growth of dendritic quartz is caused by crystallization at a minimum undercooling of 55°C. The origin of the ΔT by thermal or constitutional supercooling does not appear to affect the form of the dendrites. Quartz dendrites are formed from silicate liquids in the comparatively simple ternary system $NaAlSi_3O_8$-SiO_2-H_2O regardless of the crystallization sequence of feldspar and quartz. Dendrite development does not show any relation to the presence or absence of a H_2O-rich vapor phase. Crystallization of quartz dendrites in more complex synthetic and natural systems is also unrelated to crystallization sequence. Dendrites grow equally well in materials from the Harding pegmatite (Fenn, 1986) in which quartz is the liquidus phase and in compositions in the haplogranite system (Swanson, 1977) in which quartz crystallization follows plagioclase. Pressure does not seem to be an important variable that directly controls growth of quartz dendrites. Results presented here show uniform patterns of dendrite development over the pressure range 2–8 kbar. Thus, quartz dendrite development appears unrelated to any unique bulk composition or pressure range, but instead depends upon crystallization at some undercooled condition.

Unique geologic conditions are required to produce undercooled conditions that promote formation of dendritic quartz. Subvolcanic environments sometimes provide rapid temperature fluctuations resulting in undercoolings that favor development of dendritic quartz. Resorption textures in quartz that are often reported from hypabyssal rocks should be carefully examined to determine the origin of the dendritic crystal form. Rapid crystal growth in pegmatitic environments may produce significant undercoolings along crystal-melt interfaces related to constitutional supercooling. Dendritic quartz crystallizing in this local zone of undercooling may explain at least some of the graphic texture often found in these systems.

Acknowledgments

This research has benefited greatly from the interest, stimulation, and encouragement of Dick Jahns. During a trip through the Spruce Pine pegmatite district in 1978, Dick pointed us toward critical field relations (based on his earlier mapping) that helped us understand how undercooling in our experiments could relate to natural plutonic systems. We will miss the insight that Dick provided and his special ability to relate field and experimental studies.

The late Peter R. Gordon provided technical assistance and advice during the investigation. With his passing we have lost a real friend. Experiments were done at Stanford University and were funded by National Science Foundation grants GA41731 (to W. C. Luth, G. E. Brown, and W. A. Tiller), EAR74-0356-A01 (to G. E. Brown, W. A. Tiller, and P. M. Fenn) and EAR76-22688 to R. H. Jahns and P. M. Fenn). Discussions with W. C. Luth, R. H. Jahns, P. E. Long, and M. P. Taylor were quite helpful at various stages of the study. D. S. Barker, D. C. Presnall, M. T. Naney, B. M. Walker, R. J. Kirkpatrick, and G. E. Lofgren reviewed an earlier version of this manuscript, and many of their helpful comments have been incorporated into the present draft. Bruce Walker, Climax Molybdenum Company, supplied photographs of dendritic quartz in the Henderson stocks.

References

Barker, D.S. (1970) Composition of granophyre, myrmekite, and graphic granite. Geological Society of America Bulletin, 81, 3339–3350.

Brown, S.D., and Kistler, S.S. (1959) Devitrification of high-SiO_2 glasses in the system Al_2O_3-SiO_2. American Ceramic Society Journal, 42, 263–270.

Cameron, E.N., Jahns, R.H., McNair, A.H., and Page, L.R. (1949) Internal structure of granitic pegmatites. Economic Geology Monograph 2.

Christensen, N.H., Cooper, A.R., and Rawal, B.S. (1973) Kinetics of dendritic precipitation of cristobalite from a potassium silicate melt. American Ceramic Society Journal, 56, 557–561.

Fenn, P.M. (1977) The nucleation and growth of alkali feldspars from hydrous melts. Canadian Mineralogist, 15, 135–161.

——— (1986) On the origin of graphic granite. American Mineralogist, 71, 325–330.
Fenner, C.N. (1913) The stability relation of the silica minerals. American Journal of Science, 186, 331–384.
Jahns, R.H. (1955) The study of pegmatites. Economic Geology, 50, 1025–1130.
Keith H.D., and Padden, F.J., Jr. (1963) A phenomenological theory of spherulite crystallization. Journal of Applied Physics, 34, 2409–2421.
Kirkpatrick, R. J. (1975) Crystal growth from the melt: A review. American Mineralogist, 60, 798–814.
——— (1981) Kinetics of crystallization of igneous rocks. In A.C. Lasaga and R.J. Kirkpatrick, Eds. Kinetics of geochemical processes, 321–398. Mineralogical Society of America Reviews in Mineralogy, 8.
Kushiro, Ikuo. (1976) Changes in viscosity and structure of melt of $NaAlSi_2O_6$ composition at high pressure. Journal of Geophysical Research, 81, 6347–6356.
Lofgren, G.E. (1971) Experimentally produced devitrification textures in natural rhyolite glass. Geological Society of America Bulletin, 82, 111–124.
Luth, W.C. (1969) The systems $NaAlSi_3O_8$-SiO_2 and $KAlSi_3O_8$-SiO_2 to 20 kb and the relationship between H_2O content, P_{H_2O} and P_{total} in granitic magmas. American Journal of Science, 267A, 325–341.
Luth, W.C., and Ingamells, C.O. (1965) Gel preparation of starting materials for hydrothermal experimentation. American Mineralogist, 50, 255–258.
Luth, W.C., Jahns, R.H., and Tuttle, O.F. (1964) The granite system at pressures of 4 to 10 kilobars. Journal of Geophysical Research, 69, 759–773.
Maurice, C.S. (1940) The pegmatites of the Spruce Pine district, North Carolina. Economic Geology, 35, 49–78, 158–187.
Mustart, D.A. (1972) Phase relations in the peralkaline portion of the system Na_2O-Al_2O_3-SiO_2-H_2O. Ph.D. thesis, Stanford University, Stanford, California.
O'Hara, S., Tarshis, L.A., Tiller, W.A., and Hunt, J.P. (1968) Discussion of interface stability of large facets on solution grown crystals. Journal of Crystal Growth, 3–4, 555–561.
Petersen, J.S., and Lofgren, G.E. (1986) Lamellar and patchy intergrowth in feldspars: Experimental crystallization of eutectic silicates. American Mineralogist, 71, 343–355.
Shannon, J.R., Walker, B.M., Carten, R.B., and Geraghty, E.P. (1982) Unidirectional solidification textures and their significance in determining relative ages of intrusions at the Henderson mine, Colorado: Geology, 10, 293–297.
Shaw, H.R. (1972) Viscosities of magmatic silicate liquids: An empirical method of prediction. American Journal of Science, 272, 870–893.
Swanson, S.E. (1977) Relation of nucleation and crystal growth rate to the development of granitic textures. American Mineralogist, 62, 966–978.
——— (1978a) Morphology of quartz and alkali feldspar from the McKinney mine, Spruce Pine district, North Carolina. (abs.) EOS (Transactions of the American Geophysical Union), 59, 396.
——— (1978b) Snowflake-like quartz, McKinney mine, North Carolina—Evidence for rapid crystallization. Geological Society of America Abstracts with Programs, 10, 199.
——— (1979) The effect of CO_2 on phase equilibria and crystal growth in the system $KAlSi_3O_8$-$NaAlSi_3O_8$-$CaAl_2Si_2O_8$-SiO_2-H_2O-CO_2 to 8000 bars. American Journal of Science, 279, 703–720.
Tuttle, O.F., and Bowen, N.L. (1958) Origin of granite in the light of experimental studies. Geological Society of America Memoir 74.
Wagstaff, F.E. (1968) Crystallization kinetics of internally nucleated vitreous silica. American Ceramic Society Journal, 51, 449–452.
——— (1969) Crystallization and melting kinetics of cristobalite. American Ceramic Society Journal, 52, 650–654.
White, W.H., Bookstrom, A.A., Kamilli, R.J., Ganster, M.W., Smith, R.P., Ranta, D.E., and Steininger, R.C. (1981) Character and origin of Climax-type molybdenum deposits: Economic Geology, 75th Anniversary Volume, 270–316.
Whitney, J.A. (1975) The effects of pressure, temperature and X_{H_2O} on phase assemblage in four synthetic rock compositions. Journal of Geology, 83, 1–31.

Manuscript received April 8, 1985
Manuscript accepted October 11, 1985